Dynamic Modeling and Adaptive VSC of Two-Link Flexible Manipulators Using a Hybrid Sliding Surface

Wen-Jun Cao[1] and Jian-Xin Xu[2]

Abstract

To suppress the resonance modes of flexible manipulator and to expedite the convergence, a hybrid sliding mode consisting of Frequency Shaped Optimal Sliding Mode (FSOSM) and Terminal Sliding Mode (TSM) is proposed and applied to two-link flexible manipulator, which is an extension of our previous work [1]. An Adaptive Variable Structure Control (AVSC) is designed to estimate the upper bounds on the norm of uncertainties. The adaptation law generates a relatively small gain in the initial stage to reduce the impact to the system and a higher gain at the equilibrium to lower steady state error. Dead zone scheme is introduced to further improve system robustness. Attractiveness of the dead zone for the proposed AVSC is proven. Simulation results demonstrate the effectiveness of the proposed method.

Keywords: Multi-link Flexible Manipulator, Variable Structure Control, Adaptive Estimation, Dead Zone, Frequency Shaped Optimal Sliding Mode, Terminal Sliding Mode, Lyapunov Direct Method, Chattering Elimination.

1 Dynamic Formulation

In this paper, a clamped-loaded Euler-Bernoulli beam is selected as the approximate model for each flexible link illustrated in Figure 1. By the assumed-mode approach, the beam under free vibration is supposed to contain r finite dominant modes. The deformation is expressed as $y_i(x_i,t) = \boldsymbol{\phi}_i^T(x_i)\mathbf{q}_i(t)$ where $\boldsymbol{\phi}_i = [\phi_{i1}, \phi_{i2}, \cdots, \phi_{ir}]^T$, $\mathbf{q}_i = [q_{i1}, q_{i2}, \cdots, q_{ir}]^T$, $i = 1, 2$. l_i, m_i, E_iI_i, ρ_i, A_i, τ_i, θ_i, μ_i and J_{ih} are the length, mass, flexural rigidity, volume density, cross-sectional area, control torque, rigid angular displacement, elastic damping coefficient and actuator's moment of inertia of the ith flexible beam. m_{1t} is the mass of the actuator at O' and M_t is the mass of payload. Using Lagrangian approach, once the total kinetic energy, potential energy and Raleigh dissipation function are determined, we derived the dynamic equation of two-link flexible manipulators laboriously

$$\begin{bmatrix} M_{RR}(\boldsymbol{\xi}) & M_{RF}(\boldsymbol{\xi}) \\ M_{RF}^T(\boldsymbol{\xi}) & M_{FF}(\boldsymbol{\xi}) \end{bmatrix} \begin{bmatrix} \ddot{\boldsymbol{\theta}} \\ \ddot{\mathbf{q}} \end{bmatrix} + \begin{bmatrix} \mathbf{0} & \mathbf{0} \\ \mathbf{0} & D_F \end{bmatrix} \begin{bmatrix} \dot{\boldsymbol{\theta}} \\ \dot{\mathbf{q}} \end{bmatrix} + \begin{bmatrix} \mathbf{0} & \mathbf{0} \\ \mathbf{0} & C_F \end{bmatrix} \begin{bmatrix} \boldsymbol{\theta} \\ \mathbf{q} \end{bmatrix} + \begin{bmatrix} \mathbf{h}_R(\boldsymbol{\xi}, \dot{\boldsymbol{\xi}}) \\ \mathbf{h}_F(\boldsymbol{\xi}, \dot{\boldsymbol{\xi}}) \end{bmatrix} = \begin{bmatrix} \boldsymbol{\tau} + \mathbf{d} \\ \mathbf{0} \end{bmatrix} \quad (1)$$

where

$$\boldsymbol{\tau} = \begin{bmatrix} \tau_1 & \tau_2 \end{bmatrix}^T,\ \boldsymbol{\xi} = \begin{bmatrix} \boldsymbol{\theta}^T & \mathbf{q}^T \end{bmatrix}^T,$$

$$\boldsymbol{\theta} = \begin{bmatrix} \theta_1 & \theta_2 \end{bmatrix}^T,\ \mathbf{q} = \begin{bmatrix} \mathbf{q}_1^T & \mathbf{q}_2^T \end{bmatrix}^T,$$

$$M_{RR} = \begin{bmatrix} m_{11} & m_{12} \\ m_{12} & m_{22} \end{bmatrix}, M_{RF} = \begin{bmatrix} \mathbf{m}_{13} & \mathbf{m}_{14} \\ \mathbf{m}_{23} & \mathbf{m}_{24} \end{bmatrix},$$

$$M_{FF} = \begin{bmatrix} M_{33} & M_{34} \\ M_{34}^T & M_{44} \end{bmatrix},$$

$$m_{11} = J_{1h} + \frac{1}{3}m_1l_1^2 + (m_{1t} + M_t + m_2)l_1^2 + \mathbf{q}_1^T\left[\int_0^{l_1}\rho_1A_1\boldsymbol{\Phi}_1\boldsymbol{\Phi}_1^T dx_1 + (m_{1t} + M_t + m_2)\boldsymbol{\Phi}_{1e}\boldsymbol{\Phi}_{1e}^T\right]\mathbf{q}_1 + \frac{1}{3}m_2l_2^2 + M_tl_2^2 + 2l_1cos\theta_2\left(\frac{1}{2}m_2 + M_t\right)l_2 + \mathbf{q}_2^T\left[\int_0^{l_2}\rho_2A_2\boldsymbol{\Phi}_2\boldsymbol{\Phi}_2^T dx_2 + M_t\boldsymbol{\Phi}_{2e}\boldsymbol{\Phi}_{2e}^T\right]\mathbf{q}_2 - 2l_1sin\theta_2\left(\int_0^{l_2}\rho_2A_2\boldsymbol{\Phi}_2^T dx_2 + M_t\boldsymbol{\Phi}_{2e}^T\right)\mathbf{q}_2 + 2\boldsymbol{\Phi}_{1e}^T\mathbf{q}_1sin\theta_2\left(\frac{1}{2}m_2 + M_t\right)l_2,$$

$$m_{12} = \frac{1}{3}m_2l_2^2 + M_tl_2^2 + l_1cos\theta_2\left(\frac{1}{2}m_2 + M_t\right)l_2 + \mathbf{q}_2^T\left[\int_0^{l_2}\rho_2A_2\boldsymbol{\Phi}_2\boldsymbol{\Phi}_2^T dx_2 + M_t\boldsymbol{\Phi}_{2e}\boldsymbol{\Phi}_{2e}^T\right]\mathbf{q}_2 - l_1sin\theta_2\left(\int_0^{l_2}\rho_2A_2\boldsymbol{\Phi}_2^T dx_2 + M_t\boldsymbol{\Phi}_{2e}^T\right)\mathbf{q}_2 + \boldsymbol{\Phi}_{1e}^T\mathbf{q}_1sin\theta_2\left(\frac{1}{2}m_2 + M_t\right)l_2,$$

$$m_{22} = J_{2h} + \frac{1}{3}m_2l_2^2 + M_tl_2^2 + \mathbf{q}_2^T\left[\int_0^{l_2}\rho_2A_2\boldsymbol{\Phi}_2\boldsymbol{\Phi}_2^T dx_2 + M_t\boldsymbol{\Phi}_{2e}\boldsymbol{\Phi}_{2e}^T\right]\mathbf{q}_2,$$

$$\mathbf{m}_{13} = \int_0^{l_1}\rho_1A_1x_1\boldsymbol{\Phi}_1^T dx_1 + (m_{1t} + M_t + m_2)l_1\boldsymbol{\Phi}_{1e}^T$$

[1]Wen-Jun Cao is with Data Storage Institute, National University of Singapore, DSI Building, 5 Engineering Drive 1, (off Kent Ridge Crescent, NUS), Singapore 117608. Tel: +65-874-8779. Fax: +65-776-6527. Email: wjcao@dsi.nus.edu.sg.

[2]Jian-Xin Xu is with the Electrical Engineering Department, National University of Singapore, 10 Kent Ridge Crescent, Singapore 119260. Tel: +65-874-2566. E-mail: elexujx@nus.edu.sg.

$$+cos\theta_2\left(\frac{1}{2}m_2+M_t\right)l_2\mathbf{\Phi}_{1e}^T$$
$$-sin\theta_2\mathbf{q}_2^T\left(\int_0^{l_2}\rho_2A_2\mathbf{\Phi}_2dx_2+M_t\mathbf{\Phi}_{2e}\right)\mathbf{\Phi}_{1e}^T,$$

$$\mathbf{m}_{14}=\int_0^{l_2}\rho_2A_2x_2\mathbf{\Phi}_2^Tdx_2+M_tl_2\mathbf{\Phi}_{2e}^T$$
$$+\mathbf{\Phi}_{1e}^T\mathbf{q}_1\left(\int_0^{l_2}\rho_2A_2\mathbf{\Phi}_2^Tdx_2+M_t\mathbf{\Phi}_{2e}^T\right)$$
$$+l_1cos\theta_2\left(\int_0^{l_2}\rho_2A_2\mathbf{\Phi}_2^Tdx_2+M_t\mathbf{\Phi}_{2e}^T\right),$$

$$\mathbf{m}_{23}=-\mathbf{q}_2^T\left(\int_0^{l_2}\rho_2A_2\mathbf{\Phi}_2dx_2+\mathbf{\Phi}_{2e}M_t\right)\mathbf{\Phi}_{1e}^Tsin\theta_2$$
$$+cos\theta_2\mathbf{\Phi}_{1e}^T\left(\frac{1}{2}m_2+M_t\right)l_2,$$

$$\mathbf{m}_{24}=\int_0^{l_2}\rho_2A_2x_2\mathbf{\Phi}_2^Tdx_2+M_tl_2\mathbf{\Phi}_{2e}^T,$$

$$M_{33}=(m_1+m_2+M_t)\mathbf{\Phi}_{1e}\mathbf{\Phi}_{1e}^T+\int_0^{l_1}\rho_1A_1\mathbf{\Phi}_1\mathbf{\Phi}_1^Tdx_1,$$

$$M_{34}=cos\theta_2\mathbf{\Phi}_{1e}\left(\int_0^{l_2}\rho_2A_2\mathbf{\Phi}_2^Tdx_2+M_t\mathbf{\Phi}_{2e}^T\right),$$

$$M_{44}=\int_0^{l_2}\rho_2A_2\mathbf{\Phi}_2\mathbf{\Phi}_2^Tdx_2+M_t\mathbf{\Phi}_{2e}\mathbf{\Phi}_{2e}^T,$$

$$C_F=\text{diag}\left[\begin{array}{cccccc}c_{11}&\cdots&c_{1r}&c_{21}&\cdots&c_{2r}\end{array}\right],$$

$$c_{ij}=E_iI_i\int_0^{l_i}\left[\frac{d\phi_{ij}(x_i)}{dx_i}\right]^2dx_i,\ i=1,2,\ j=1,\cdots,r,$$

$$D_F=\text{diag}\left[\int_0^{l_1}\mu_1\boldsymbol{\phi}_1(x_1)\boldsymbol{\phi}_1^T(x_1)dx_1,\right.$$
$$\left.\int_0^{l_2}\mu_2\boldsymbol{\phi}_2(x_2)\boldsymbol{\phi}_2^T(x_2)dx_2\right],$$

$$\mathbf{h}_R(\boldsymbol{\xi},\ \dot{\boldsymbol{\xi}})=\frac{d}{dt}M_{RR}(\boldsymbol{\xi})\dot{\boldsymbol{\theta}}+\frac{d}{dt}M_{RF}(\boldsymbol{\xi})\dot{\mathbf{q}}-\frac{1}{2}\dot{\boldsymbol{\xi}}^T\frac{\partial M(\boldsymbol{\xi})}{\partial\theta}\dot{\boldsymbol{\xi}},$$

$$\mathbf{h}_F(\boldsymbol{\xi},\ \dot{\boldsymbol{\xi}})=\frac{d}{dt}M_{RF}^T(\boldsymbol{\xi})\dot{\boldsymbol{\theta}}+\frac{d}{dt}M_{FF}(\boldsymbol{\xi})\dot{\mathbf{q}}-\frac{1}{2}\dot{\boldsymbol{\xi}}^T\frac{\partial M(\boldsymbol{\xi})}{\partial\mathbf{q}}\dot{\boldsymbol{\xi}},$$

and subscript e is used to denote the value of the variable occurring at the tip of the upper link, i.e. the value at $x_2=l_2$. $\mathbf{d}$ is the exogenous disturbance associated with control torque $\boldsymbol{\tau}$ and $\mathbf{d}=[d_1\ d_2]^T$.

2 Adaptive VSC Design

Frequency Shaped Optimal Sliding Mode (FSOSM) was originated in [2] to suppress the resonance modes. The low switching slop slows down the transient response, and the steady-state error could be rather large. Terminal Sliding Mode (TSM) [3] is characterized by an increasing equivalent switching slope as the tracking error decreases. The large switching slope expedites convergence and reduces steady-state error. To suppress the resonance modes of flexible manipulators and to expedite the convergence, a hybrid sliding mode consisting of FSOSM and TSM was originated and applied to single-link flexible manipulators in our work [1] which fully explains the motivation, formulation and property analysis of the hybrid sliding surface.

Here we extend our hybrid sliding surface to control two-link flexible manipulator. The hybrid sliding surface of the ith link of flexible manipulator is

$$\sigma_i=e_{2i}+\alpha c_{ei}e_{1i}+(1-\alpha)c_{pi}l(e_{1i})+\alpha c_{1i}z_{1i}+\alpha c_{2i}z_{2i}$$

where $i=1,2$, $e_{2i}=\dot{e}_{1i}$, $p=\frac{p_1}{p_2}$, $p_1=2m_1+1, m_1=0,1\cdots$, $p_2=2m_2+1$, $m_2=1,2\cdots$, $p_1\in\left[\frac{p_2+1}{2},p_2\right)$,

$$l(\varphi)=\left\{\begin{array}{ll}\varphi^p & |\varphi|>\varepsilon_e\\ p\varepsilon_e^{p-1}\varphi & |\varphi|\le\varepsilon_e\end{array}\right.,$$

and $\left[\begin{array}{cc}z_{1i}&z_{2i}\end{array}\right]^T$ are the states of a second-order high-pass filter. It can be rewritten into

$$\boldsymbol{\sigma}=\mathbf{e}_2+\alpha C_e\mathbf{e}_1+(1-\alpha)C_p\mathbf{l}(\mathbf{e})+\alpha H\mathbf{z}, \tag{2}$$

where $0<\alpha<1$, $\boldsymbol{\sigma}=\left[\begin{array}{cc}\sigma_1&\sigma_2\end{array}\right]^T$,
$\mathbf{e}_1=\left[\begin{array}{cc}e_{11}&e_{12}\end{array}\right]^T$, $\mathbf{e}_2=\left[\begin{array}{cc}\dot{e}_{11}&\dot{e}_{12}\end{array}\right]^T$,
$C_e=\text{diag}\left[c_{e11}\ c_{e22}\right]$, $\mathbf{z}=\left[\begin{array}{cccc}z_{11}&z_{21}&z_{12}&z_{22}\end{array}\right]^T$,
$H=\left[\begin{array}{cccc}c_{11}&c_{21}&0&0\\0&0&c_{12}&c_{22}\end{array}\right]$, $C_p=\text{diag}\left[\begin{array}{cc}c_{p1}&c_{p2}\end{array}\right]$,
$\mathbf{l}(\mathbf{e})=\left[\begin{array}{cc}l(e_{11})&l(e_{21})\end{array}\right]^T$.

The frequency shaping compensators are combined as

$$\dot{\mathbf{z}}=F\mathbf{z}+G\mathbf{e}_2$$

where

$$F=\left[\begin{array}{cccc}0&1&0&0\\-\omega_{1c}^2&-2\omega_{1c}&0&0\\0&0&0&1\\0&0&-\omega_{2c}^2&-2\omega_{2c}\end{array}\right],G=\left[\begin{array}{cc}0&0\\1&0\\0&0\\0&1\end{array}\right].$$

Denote the set point for the ith link as θ_{id}. The following can be derived from system dynamics (1) and sliding surface (2)

$$\begin{aligned}\Delta\dot{\boldsymbol{\sigma}} &= \boldsymbol{\tau}+K_1\left[\begin{array}{ccc}\dot{\theta}_1^2&\dot{\theta}_1\dot{\theta}_2&\dot{\theta}_2^2\end{array}\right]^T+K_2\left[\begin{array}{cc}\dot{\theta}_1&\dot{\theta}_2\end{array}\right]^T\\ &\quad +K_3\left[\begin{array}{cccc}z_{11}&z_{21}&z_{12}&z_{22}\end{array}\right]^T\\ &\quad +K_4+(1-\alpha)PC_pL_D\mathbf{e}_2\\ &= \boldsymbol{\tau}+K^T\boldsymbol{\chi}+(1-\alpha)PC_pL_D\mathbf{e}_2\end{aligned} \tag{3}$$

where K is given in **Appendix** and

$$\begin{aligned}\Delta &\triangleq M_{RR}-M_{RF}M_{FF}^{-1}M_{RF}^T,\\ \boldsymbol{\chi} &= \left[\dot{\theta}_1^2,\ \dot{\theta}_1\dot{\theta}_2,\ \dot{\theta}_2^2,\ \dot{\theta}_1,\ \dot{\theta}_2,\ z_{11},z_{21},z_{12},z_{22},1\right]^T,\\ P &= \text{diag}[p_1,\ p_2],\\ L_D &= \text{diag}[\dot{l}(e_{11}),\ \dot{l}(e_{12})],\\ \dot{l}(e_{1i}) &= \left\{\begin{array}{ll}e_{1i}^{p_i-1}\dot{\theta}_i & |e_{1i}|>\varepsilon_{ei}\\ \varepsilon_{ei}^{p_i-1}\dot{\theta}_i & |e_{1i}|\le\varepsilon_{ei}\end{array}\right..\end{aligned}$$

Lemma 1 [4]. *The following linear matrix inequality*

$$\begin{bmatrix} Q(\mathbf{x}) & S(\mathbf{x}) \\ S^T(\mathbf{x}) & R(\mathbf{x}) \end{bmatrix} > 0.$$

where $Q(\mathbf{x}) = Q^T(\mathbf{x})$, $R(\mathbf{x}) = R^T(\mathbf{x})$ and $S(\mathbf{x})$ depends affinely on $\mathbf{x}$, is equivalent to

$$R(\mathbf{x}) > 0,\ Q(\mathbf{x}) - S(\mathbf{x})R^{-1}(\mathbf{x})S^T(\mathbf{x}) > 0.$$

Lemma 2 *For the flexible manipulator system (1) where only finite number of flexible modes are considered, Δ is positive-definite, and $\mathbf{q}_1$, $\mathbf{q}_2$, $\dot{\mathbf{q}}_1$ and $\dot{\mathbf{q}}_2$ are all bounded.*

Proof: Since $\begin{bmatrix} M_{RR} & M_{RF} \\ M_{RF}^T & M_{FF} \end{bmatrix}$ in (1) is an *inertia matrix* and hence positive-definite. According to Lemma 1, straightforwardly we have $M_{FF} > 0$, $\Delta = M_{RR} - M_{RF}M_{FF}^{-1}M_{RF}^T > 0$. From the dynamics of the system (1), $\mathbf{q}_1$ and $\mathbf{q}_2$ are bounded to ensure that $m_{11} > 0$ and $m_{22} > 0$, and the flexible system has a finite inertia. As we consider only finite number of flexible modes in the truncated model (1), the boundedness of $\mathbf{q}_1$ and $\mathbf{q}_2$ ensures that $\dot{\mathbf{q}}_1$ and $\dot{\mathbf{q}}_2$ are all bounded. ■

From the dynamics of the system (1), it is found that Δ depends on θ_2, $\mathbf{q}$, $\dot{\mathbf{q}}$ and system parameters m_t, m_i, l_i, μ_i, J_{ih}. Define $\lambda_{max}(\Delta)$ as

$$\lambda_{max}(\Delta) = \sup_{\theta_2,\ \mathbf{q},\ \dot{\mathbf{q}},\ m_t,\ m_i,\ l_i,\ \mu_i,\ J_{ih}} \left[\max_j\ \lambda_j(\Delta)\right]$$

where $i = 1, 2$ and $j = 1, 2$. Denoting

$$|\mathbf{w}|_1 \triangleq [|w_1|\ |w_2|\ \cdots\ |w_n|]^T,$$

one obtains the following conventional VSC law

$$\boldsymbol{\tau} = -(1-\alpha)\,PC_pL_D\mathbf{e}_2 - \mathrm{sgn}(\boldsymbol{\sigma})\left\{\hat{K}_{10\times 2}^T|\boldsymbol{\chi}|_1 + \boldsymbol{\delta}\right\} \quad (4)$$

where

$$\begin{aligned}
\hat{K} &= \begin{bmatrix} \hat{\mathbf{k}}_1 & \hat{\mathbf{k}}_2 \end{bmatrix} \\
&= \begin{bmatrix} \hat{k}_{11} & \hat{k}_{12} & \cdots & \hat{k}_{19} & \hat{k}_{1a} \\ \hat{k}_{21} & \hat{k}_{22} & \cdots & \hat{k}_{29} & \hat{k}_{2a} \end{bmatrix}^T, \\
\hat{k}_{18} &= \hat{k}_{19} = \hat{k}_{26} = \hat{k}_{27} \equiv 0, \\
\mathrm{sgn}(\boldsymbol{\sigma}) &= \mathrm{diag}\begin{bmatrix} \mathrm{sgn}(\sigma_1) & \mathrm{sgn}(\sigma_2) \end{bmatrix}, \\
\boldsymbol{\delta} &= \begin{bmatrix} \delta_1 & \delta_2 \end{bmatrix}^T,\ \delta_1 > 0,\ \delta_2 > 0, \\
K_a &= \lambda_{max}(\Delta)K\Delta^{-1},\ K_a = [k_{aij}], \hat{K} = [\hat{k}_{ij}] \\
K^* &= [k_{ij}^*],\ k_{ij}^* = \sup k_{aij},\ \hat{k}_{ij} \geq k_{ij}^*. \qquad (5)
\end{aligned}$$

Theorem 1: For the system (1), the control law (4) ensures that sliding surface $\boldsymbol{\sigma}(t) = 0$ can be reached in a finite time.

Proof: Consider the following Lyapunov candidate

$$V = \frac{1}{2}\lambda_{max}(\Delta)\boldsymbol{\sigma}^T\boldsymbol{\sigma}.$$

Taking the time derivative of V and using relation (3), control law (4) and inequality (5) obtain

$$\begin{aligned}
\dot{V} &= \lambda_{max}(\Delta)\boldsymbol{\sigma}^T\Delta^{-1}\Delta\dot{\boldsymbol{\sigma}} \\
&= \lambda_{max}(\Delta)\boldsymbol{\sigma}^T\Delta^{-1}\left\{-\mathrm{sgn}(\boldsymbol{\sigma})\left[\hat{K}^T|\boldsymbol{\chi}|_1 + \boldsymbol{\delta}\right] + K^T\boldsymbol{\chi}\right\} \\
&= -\lambda_{max}(\Delta)\left[\boldsymbol{\sigma}^T\Delta^{-1}\mathrm{sgn}(\boldsymbol{\sigma})\hat{K}^T|\boldsymbol{\chi}|_1\right. \\
&\qquad \left. +\boldsymbol{\sigma}^T\Delta^{-1}\mathrm{sgn}(\boldsymbol{\sigma})\boldsymbol{\delta} - \boldsymbol{\sigma}^T\Delta^{-1}K^T\boldsymbol{\chi}\right].
\end{aligned}$$

Since Δ^{-1} is Hermitian positive-definite,

$$\begin{aligned}
\boldsymbol{\sigma}^T\Delta^{-1}\mathrm{sgn}(\boldsymbol{\sigma})\hat{K}^T|\boldsymbol{\chi}|_1 &\geq \frac{1}{\lambda_{max}(\Delta)}|\boldsymbol{\sigma}|_1^T\hat{K}^T|\boldsymbol{\chi}|_1, \\
\boldsymbol{\sigma}^T\Delta^{-1}\mathrm{sgn}(\boldsymbol{\sigma})\boldsymbol{\delta} &\geq \frac{1}{\lambda_{max}(\Delta)}|\boldsymbol{\sigma}|_1^T\boldsymbol{\delta}.
\end{aligned}$$

Using the above and (5) we have

$$\begin{aligned}
\dot{V} &\leq -|\boldsymbol{\sigma}|_1^T\hat{K}^T|\boldsymbol{\chi}|_1 + \boldsymbol{\sigma}^T\lambda_{max}(\Delta)\Delta^{-1}K^T\boldsymbol{\chi} - |\boldsymbol{\sigma}|_1^T\boldsymbol{\delta} \\
&= -|\boldsymbol{\sigma}|_1^T\hat{K}^T|\boldsymbol{\chi}|_1 + \boldsymbol{\sigma}^TK_a^T\boldsymbol{\chi} - |\boldsymbol{\sigma}|_1^T\boldsymbol{\delta} \leq -|\boldsymbol{\sigma}|_1^T\boldsymbol{\delta}.
\end{aligned}$$

The sliding condition is satisfied and sliding surface $\boldsymbol{\sigma}(t) = 0$ can be reached in a finite time. ■

From the dynamics of the system, it is found that k_{aij} depends upon $\theta_2, \mathbf{q}_1, \dot{\mathbf{q}}_1, \mathbf{q}_2, \dot{\mathbf{q}}_2, \mathbf{d}$ and system parameters m_{1t}, M_t, m_i, l_i, μ_i, J_{ih}. The perturbation bounds for system parameters are assumed to be known. θ_2 is bounded and componentwise in $[0, 2\pi]$. According to **Lemma 2**, $\mathbf{q}_1$, $\mathbf{q}_2$, $\dot{\mathbf{q}}_1$, $\dot{\mathbf{q}}_2$ are all bounded. To implement a VSC, estimation for K^*, the upper bound of K_a, must be made. In practice, however, a suitable estimation for K^* is difficult as we are not able to anticipate the variation bounds of $\theta_2, \mathbf{q}_1, \mathbf{q}_2, \dot{\mathbf{q}}_1$ and $\dot{\mathbf{q}}_2$. Overestimation may result in unnecessarily high gains and large chattering which degrade system performance. Underestimation, on the other hand, is not permitted as it may lead to instability. To alleviate the difficulty arising from making conjectural data for flexible modes, parameter variations, disturbance and other system uncertainties, an adaptation law for estimating K^* is proposed. It takes the following form

$$\dot{\hat{K}}_{10\times 2} = \gamma|\boldsymbol{\chi}|_1|\boldsymbol{\sigma}|_1^T,\ \hat{K}\ |_{t=0} = \mathbf{0}_{10\times 2}. \qquad (6)$$

Another advantage for using the above adaptive estimation is that the feedback gain $\hat{K}$ can be set to be zero at the initial stage. In the sequel, the small $\hat{K}$ in the initial stage reduces the impact to the system. On the contrary, the increasing gain when approaching the equilibrium can lower steady-state error.

Theorem 3: For the system (1), the control law (4) with adaptation law (6) ensures that $\hat{K}$ and $|\boldsymbol{\chi}|_1$ are bounded and

$$\lim_{t\to\infty}\boldsymbol{\sigma}(t) = 0.$$

Proof: Define the estimation error $\Phi = \hat{K} - K^*$ and consider the following Lyapunov function

$$V(\boldsymbol{\sigma},\ \Phi) = \frac{1}{2}\lambda_{max}(\Delta)\boldsymbol{\sigma}^T\boldsymbol{\sigma} + \frac{1}{2}\gamma^{-1}trace\left[\Phi\Phi^T\right].$$

Differentiating the above with respect to time once and using equation (3), control law (4) and adaptation law (6) yield

$$\begin{aligned}
\dot{V} &= \lambda_{max}(\Delta)\boldsymbol{\sigma}^T\Delta^{-1}\left[\boldsymbol{\tau} + (1-\alpha)\,PC_pL_D\mathbf{e}_2\right. \\
&\quad \left. + K^T\boldsymbol{\chi}\right] + \gamma^{-1}trace\left[(\hat{K} - K^*)\dot{\hat{K}}^T\right] \\
&\leq -|\boldsymbol{\sigma}|_1^T\hat{K}^T|\boldsymbol{\chi}|_1 + \boldsymbol{\sigma}^TK_a^T\boldsymbol{\chi} - |\boldsymbol{\sigma}|_1^T\boldsymbol{\delta} \\
&\quad + |\boldsymbol{\sigma}|_1^T\hat{K}^T|\boldsymbol{\chi}|_1 - |\boldsymbol{\sigma}|_1^TK^{*T}|\boldsymbol{\chi}|_1 \\
&= \boldsymbol{\sigma}^TK_a^T\boldsymbol{\chi} - |\boldsymbol{\sigma}|_1^TK^{*T}|\boldsymbol{\chi}|_1 - |\boldsymbol{\sigma}|_1^T\boldsymbol{\delta} \\
&\leq -|\boldsymbol{\sigma}|_1^T\boldsymbol{\delta} \qquad (7)
\end{aligned}$$

which is negative-definite if $\boldsymbol{\sigma} \neq \mathbf{0}_{2\times 1}$. This shows $\dot{V}$ is negative semidefinite in the $(\boldsymbol{\sigma},\ \Phi)$ space. Therefore the boundedness of V, σ_i and $\hat{K}$ are ensured and $\sigma_i \in L^\infty$. The boundedness of σ_i implies the boundedness of z_{1i} and z_{2i}, hence $\boldsymbol{\chi}$ and $|\boldsymbol{\chi}|_1$ are bounded. Because K, $\hat{K}$, $\boldsymbol{\chi}$, $|\boldsymbol{\chi}|_1$ and Δ are all bounded, it can be concluded from (3) and (4) that $\dot{\sigma}_i$ is bounded. The inequality (7) also means that σ_i are absolute integrable as

$$\int_0^\infty |\sigma_i|dt \leq \frac{1}{\delta_i}\left[V(0) - V(\infty)\right]$$

i.e., $\sigma_i \in L^1$. Since $\sigma_i \in L^1 \cap L^\infty$, $\sigma_i \in L^2$ [5]. Finally, $\sigma_i \in L^2 \cap L^\infty$ and the boundedness of $\dot{\sigma}_i$ conclude that $\lim_{t\to\infty}\sigma_i(t) = 0$. [6]. ■

3 Adaptive Variable Structure Controller with Dead Zone Scheme

The adaptive variable structure controller proposed in the previous section has two potential problems: (1) The adaptation law (6) is a positive integration process. In practical implementation, $\boldsymbol{\sigma} = \mathbf{0}$ can hardly be reached due to the presence of system perturbations and limited sampling rate. These residues in $\boldsymbol{\sigma}$, though small, will keep the adaptation integration going on and eventually lead to very high gains or even instability. (2) The control law (4) is discontinuous crossing switching surface $\boldsymbol{\sigma} = 0$ due to the $\mathrm{sgn}(\boldsymbol{\sigma})$ term. This characteristic may induce the undesirable chattering problem.

Considering the fact that system perturbations are very small nearby the equilibrium, we introduce the dead zone scheme to shut the adaptation mechanism off when switching surface enters a sufficiently small bound. To overcome the second drawback , saturation function is used to replace the signum function, and the saturation boundary layer is chosen to be consistent with the dead zone. The revised scheme is given below:

$$\begin{aligned}
\boldsymbol{\tau} &= -(1-\alpha)\,PC_pL_D\mathbf{e}_2 \\
&\quad -\mathrm{sat}(\boldsymbol{\sigma})\left\{\hat{K}_{10\times 2}|\boldsymbol{\chi}|_1 + \boldsymbol{\delta}\right\}, \quad (8) \\
\dot{\hat{K}}_{10\times 2} &= \begin{cases} \gamma|\boldsymbol{\chi}|_1|\boldsymbol{\sigma}|_1^T & \boldsymbol{\sigma}^T\boldsymbol{\sigma} > \boldsymbol{\varepsilon}^T\boldsymbol{\varepsilon} \\ \mathbf{0}_{10\times 2} & \boldsymbol{\sigma}^T\boldsymbol{\sigma} \leq \boldsymbol{\varepsilon}^T\boldsymbol{\varepsilon} \end{cases} \qquad (9)
\end{aligned}$$

where $i = 1, 2$, $\boldsymbol{\varepsilon} = \begin{bmatrix} \varepsilon_1 & \varepsilon_2 \end{bmatrix}^T$,

$$\begin{aligned}
\mathrm{sat}(\boldsymbol{\sigma}) &= \mathrm{diag}\begin{bmatrix} \mathrm{sat}(\sigma_1,\ \varepsilon_1) & \mathrm{sat}(\sigma_2,\ \varepsilon_2) \end{bmatrix}, \\
\mathrm{sat}(\sigma_i,\ \varepsilon_i) &= \begin{cases} sign(\sigma_i) & |\sigma_1| > \varepsilon_1 \ or\ |\sigma_2| > \varepsilon_2 \\ \sigma_i/\varepsilon_i & |\sigma_1| \leq \varepsilon_1 \ and\ |\sigma_2| \leq \varepsilon_2 \end{cases}.
\end{aligned}$$

The size of dead zone is defined by $\sqrt{\boldsymbol{\varepsilon}^T\boldsymbol{\varepsilon}}$.

Theorem 3: For the system (1), the control law (8) and adaptation law (9) make the dead zone $\left\{E_0 \mid \boldsymbol{\sigma}^T\boldsymbol{\sigma} \leq \boldsymbol{\varepsilon}^T\boldsymbol{\varepsilon}\right\}$ be an attractive region. Any system state lies outside the region will reach and enter it at some *finite* time. Moreover, system states will stay inside dead zone permanently eventually.

Proof: Define Ω_1, Ω_2 as

$$\Omega_1 \triangleq \left\{t \mid \boldsymbol{\sigma}^T\boldsymbol{\sigma} \leq \boldsymbol{\varepsilon}^T\boldsymbol{\varepsilon}\right\},\ \Omega_2 \triangleq \left\{t \mid \boldsymbol{\sigma}^T\boldsymbol{\sigma} > \boldsymbol{\varepsilon}^T\boldsymbol{\varepsilon}\right\}$$

so that $\Omega_1 \cup \Omega_2 = R^+$. Consider the following Lyapunov function $V(\sigma,\ \Phi)$

$$= \begin{cases} \frac{1}{2}\lambda_{max}(\Delta)\boldsymbol{\sigma}^T\boldsymbol{\sigma} + \frac{1}{2}\gamma^{-1}trace\left[\Phi^T\Phi\right] & t \in \Omega_2 \\ \frac{1}{2}\lambda_{max}(\Delta)\boldsymbol{\varepsilon}^T\boldsymbol{\varepsilon} + \frac{1}{2}\gamma^{-1}trace\left[\Phi^T\Phi\right] & t \in \Omega_1 \end{cases}.$$

Note that $V(\sigma,\ \Phi) \geq \frac{1}{2}\boldsymbol{\varepsilon}^T\boldsymbol{\varepsilon} > 0$; $V(\sigma,\ \Phi)$ is continuous in the $(\sigma,\ \Phi)$ space and $\dot{V} = 0$ for $t \in \Omega_1$. When $t \in \Omega_2$, system states stay outside the dead zone and $\boldsymbol{\sigma}^T\boldsymbol{\sigma} > \boldsymbol{\varepsilon}^T\boldsymbol{\varepsilon}$, the control law (8) is the same as (4). In term of (7), $\dot{V} \leq -|\boldsymbol{\sigma}|_1^T\boldsymbol{\delta}$. Since

$$|\boldsymbol{\sigma}|_1^T\boldsymbol{\delta} = |\sigma_1|\delta_1 + |\sigma_2|\delta_2 \geq \min_i\ \varepsilon_i\delta_i,\ i = 1,\ 2,$$

then

$$\dot{V} \leq -\min_i \varepsilon_i\delta_i < 0,\ t \in \Omega_2. \qquad (10)$$

The negative definiteness of $\dot{V}$ results a *finite* time to reach dead zone and the total time during which adaptation takes place is *finite*.

Due to system perturbations, it is possible that system states leave E_0 at some time t_1. As a result of (10), the controller law and adaptation law will drive the states to re-enter dead zone at a *finite* time $t_2 > t_1$. Integration of (10) from t_1 to t_2 gives

$$V(t_2) \leq V(t_1) - \min_i \varepsilon_i\delta_i\Delta t_1,\ \Delta t_1 = t_2 - t_1.$$

Assume that the system states move out of E_0 at time t_3 again and re-enter it at t_4. In general, system states

leave dead zone at t_{2n-1} and re-enter at t_{2n}. Now let us show that such motion can only repeat for *finite* times ($n < \infty$) and system states will stay within the dead zone E_0 forever. For an arbitrary number n, the following stands

$$\begin{aligned} V(t_{2n}) &\leq V(t_{2n-1}) - \min_i \varepsilon_i \delta_i \Delta t_n \leq \cdots\cdots \\ &\leq V(t_1) - \sum_{j=0}^{n-1} \min_i \varepsilon_i \delta_i \Delta t_{n-j}, \end{aligned}$$

where $\Delta t_{n-j} = t_{2n-2j} - t_{2n-2j-1}$. Since $V(t_1)$, ε_i and $\delta_i > 0$ are all finite positive constants, and $V(t_{2n})$ is positive definite, we have

$$\sum_{j=0}^{n-1} \Delta t_{n-j} \leq \frac{V(t_1)}{\min_i \varepsilon_i \delta_i} < \infty$$

Hence $\Delta t_n \to 0$ as $n \to \infty$, i.e., the system states stay inside E_0 forever eventually. ■

4 Case Study

To demonstrate the effectiveness of the proposed method, a case study on a two-link flexible manipulator is conducted. The beam is constructed from Aluminum with a rectangular cross-sectional area. The first four flexible modes are considered for each flexible link. The physical parameters are: $l_1 = l_2 = 1\ m$, $E_1 I_1 = E_2 I_2 = 68.04\ Nm^2$, $m_1 = m_2 = 0.5859\ Kg$, $\mu = 0.01$, the lowest resonance frequency is $5.89\ rad/s$.

To apply FSOSM, ω_c and a of the second-order filter for both links are chosen to be $5\ rad/sec$ and 10 respectively. This ensures a $40\ db$ roll-off rate for any frequency above ω_c that is lower than the lowest natural frequency of the links. The initial positions of the lower and upper link are identically at $45°$. The commanded final position for the lower and upper link are 90^o and 0^o respectively. FSOSM for the ith link with the above mentioned second-order filter is calculated to be $\sigma_i = \dot{e}_i + 0.01 e_i + 24.1893 z_{1i} + 8.4864 z_{2i}$. TSM for the ith link is chosen to be $\sigma_i = \dot{e}_i + 1.5 e_i^{\frac{3}{5}}$. The derivations of adaptive VSC for the FSOSM and TSM cases are similar to the controller design for the hybrid sliding mode case by choosing $\alpha = 1$ and $\alpha = 0$ respectively. The hybrid sliding surface for the ith link is chosen by setting $\alpha = 0.8$ as

$$\sigma_i = \dot{e}_i + 0.008 e_i + 0.3 l(e_i^{\frac{3}{5}}) - 19.35144 z_{1i} - 6.78912 z_{2i}.$$

As the extra DOFs provided by $z_{1i}(t)$ and $z_{2i}(t)$, reaching phase is eliminated by choosing

$$[z_{1i}(0),\ z_{2i}(0)]^T = \left[\ 0,\quad \tfrac{0.008}{6.78912} e_i(0) + \tfrac{0.3}{6.78912} e_i^{\frac{3}{5}}(0)\ \right]^T.$$

The sampling interval is $T_s = 1\ msec$. The initial values for $\hat{\mathbf{K}}$ is set to be $\mathbf{0}_{10\times 2}$ and the adaptation gain is chosen as $\gamma = 200$. Saturation function is chosen as $\varepsilon_i = 0.05$. In simulation, the measured $\theta_i(t)$ and $\dot{\theta}_i(t)$ are contaminated by white noise $w_i(t)$ and $v_i(t)$ respectively which are normally distributed, with zero mean and variance 0.00025. To demonstrate the robustness of the system, the following disturbance $d_i(t)$ is also applied to the ith link $d_i(t) = \begin{cases} 0\ Nm & t < 1\ sec. \\ 0.1\ Nm & t \geq 1\ sec. \end{cases}$. The tip trajectory is plotted in Figure 2 for hybrid sliding mode. It was observed that tip converged more smoothly than the TSM case; it moved faster and produces smaller steady-state error than the FSOSM case. It was observed from Figure 3 and 4 that the magnitudes of control torques are small and rather smooth. Figure 5 illustrates the estimate $\hat{k}_{2a}$ versus $\boldsymbol{\sigma}^T\boldsymbol{\sigma}$ with dead zone scheme. System state enters and leaves deadzone for 3 times, then it keeps staying inside it forever.

5 Conclusion

In this paper, a hybrid sliding mode which combines FSOSM and TSM penalizes the inherent resonance mode of flexible manipulator and expedites tip convergence. An Adaptive Variable Structure Control with dead zone modification is presented. The unnecessarily high gains and serious chattering caused by overestimated system uncertainties are avoided by the proposed adaptive estimation algorithm. Dead zone introduced improves system robustness.

References

[1] J.-X. Xu and W.-J. Cao, "Synthesized sliding mode control of a single-link flexible robot," *International Journal of Control*, vol. 73, no. 3, pp. 197–209, 2000.

[2] K. D. Young and U. Ozguner, "Frequency shaping compensator design for sliding mode," *International Journal of Control*, vol. 57, pp. 1005–1019, 1993.

[3] Z. Man, A. P. Paplinkski, and H. R. Wu, "A robust mimo terminal sliding mode control scheme for rigid robotics manipulators," *IEEE Transactions on Automatic Control*, vol. 39, no. 12, pp. 2464–2469, 1994.

[4] A. Albert, "Conditions for positive and nonnegative definiteness in terms of pseudoinverses," *SIAM Journal of Applied Mathematics*, vol. 17, pp. 434–440, 1969.

[5] C. A. Desoer and M. Vidyasagar, *Feedback systems input-output properties*, Academic Press, New York, 1975.

[6] K. S. Narendra, *Stable adaptive systems*, Prenticd-Hall International, Englewood Cliffs, New Jersey, 1989.

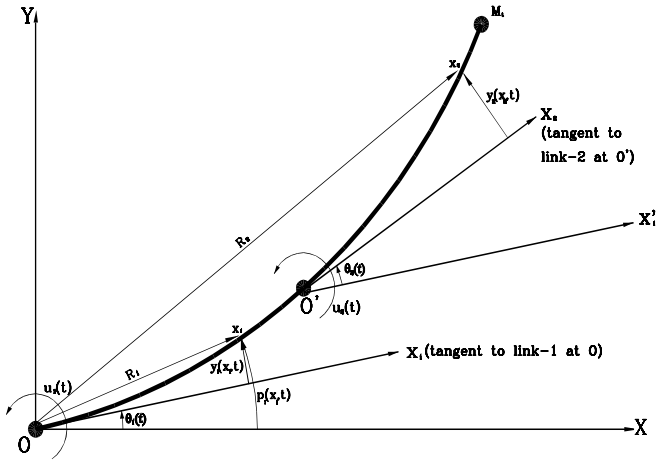

Figure 1: A two-link flexible robotic manipulator

Appendix: Derived K Matrix

$$
\begin{aligned}
K &= \left[\begin{array}{cccc} K_1 & K_2 & K_3 & K_4 \end{array}\right]^T \\
&= \left[\begin{array}{cccc} k_{11} & k_{12} & \cdots & k_{19} & k_{1a} \\ k_{21} & k_{22} & \cdots & k_{29} & k_{2a} \end{array}\right]^T, \\
k_{18} &= k_{19} = k_{26} = k_{27} \equiv 0, \\
K_1 &= M_{RF} M_{FF}^{-1} K_{f1} - K_{r1}, \\
K_2 &= M_{RF} M_{FF}^{-1} K_{f2} - K_{r2} \\
&\quad + \alpha \left[M_{RR} - M_{RF} M_{FF}^{-1} M_{RF}^T \right] (C_e + HG), \\
K_3 &= \alpha \left[M_{RR} - M_{RF} M_{FF}^{-1} M_{RF}^T \right] HF, \\
K_4 &= M_{RF} M_{FF}^{-1} \left(K_F \mathbf{q} + C_F \dot{\mathbf{q}} \right) \\
&\quad - \left[\begin{array}{c} \dot{\mathbf{q}}_2^T \frac{\partial \mathbf{m_{13}}}{\partial \mathbf{q}_2} \dot{\mathbf{q}}_1 + \dot{\mathbf{q}}_1^T \frac{\partial \mathbf{m_{14}}}{\partial \mathbf{q}_2} \dot{\mathbf{q}}_1 \\ \dot{\mathbf{q}}_2^T \frac{\partial \mathbf{m_{23}}}{\partial \mathbf{q}_2} \dot{\mathbf{q}}_1 - \dot{\mathbf{q}}_1^T \frac{\partial M_{34}}{\partial \theta_2} \dot{\mathbf{q}}_2 \end{array}\right] + \mathbf{d}, \\
K_{r1} &= \left[\begin{array}{ccc} 0 & \frac{\partial m_{11}}{\partial \theta_2} & \frac{\partial m_{12}}{\partial \theta_2} \\ -\frac{1}{2} \frac{\partial m_{11}}{\partial \theta_2} & 0 & 0 \end{array}\right], \\
K_{r2} &= \left[\begin{array}{c} \left(\frac{\partial m_{11}}{\partial \mathbf{q}_1} \right)^T \dot{\mathbf{q}}_1 + \left(\frac{\partial m_{11}}{\partial \mathbf{q}_2} \right)^T \dot{\mathbf{q}}_2 \\ \left(\frac{\partial m_{12}}{\partial \mathbf{q}_1} - \frac{\partial \mathbf{m_{13}}}{\partial \theta_2} \right)^T \dot{\mathbf{q}}_1 + \left(\frac{\partial m_{12}}{\partial \mathbf{q}_2} - \frac{\partial \mathbf{m_{14}}}{\partial \theta_2} \right)^T \dot{\mathbf{q}}_2 \\ \left(\frac{\partial m_{12}}{\partial \mathbf{q}_1} + (\frac{\partial \mathbf{m_{13}}}{\partial \theta_2} \right)^T \dot{\mathbf{q}}_1 + \left(\frac{\partial m_{12}}{\partial \mathbf{q}_2} + (\frac{\partial \mathbf{m_{14}}}{\partial \theta_2} \right)^T \dot{\mathbf{q}}_2 \\ \left(\frac{\partial m_{22}}{\partial \mathbf{q}_2} \right)^T \dot{\mathbf{q}}_2 \end{array}\right] \\
K_{f1} &= \left[\begin{array}{ccc} -\frac{1}{2} \frac{\partial m_{11}}{\partial \mathbf{q}_1} & \frac{\partial \mathbf{m}_{13}^T}{\partial \theta_2} - \frac{\partial m_{12}}{\partial \mathbf{q}_1} & \frac{\partial \mathbf{m}_{23}^T}{\partial \theta_2} \\ -\frac{1}{2} \frac{\partial m_{11}}{\partial \mathbf{q}_2} & -\frac{\partial m_{12}}{\partial \mathbf{q}_2} + \frac{\partial \mathbf{m}_{14}^T}{\partial \theta_2} & -\frac{1}{2} \frac{\partial m_{22}}{\partial \mathbf{q}_2} \end{array}\right], \\
K_{f2} &= \left[\begin{array}{ccc} \frac{\partial \mathbf{m}_{13}^T}{\partial \mathbf{q}_2} \dot{\mathbf{q}}_2 - \frac{\partial \mathbf{m_{14}}}{\partial \mathbf{q}_1} \dot{\mathbf{q}}_2 & \frac{\partial \mathbf{m}_{23}^T}{\partial \mathbf{q}_2} \dot{\mathbf{q}}_2 + \frac{\partial M_{34}}{\partial \theta_2} \dot{\mathbf{q}}_2 \\ \frac{\partial \mathbf{m}_{14}^T}{\partial \mathbf{q}_1} \dot{\mathbf{q}}_1 - \frac{\partial \mathbf{m_{13}}}{\partial \mathbf{q}_2} \dot{\mathbf{q}}_1 & \frac{\partial M_{34}^T}{\partial \theta_2} \dot{\mathbf{q}}_1 - \frac{\partial \mathbf{m_{23}}}{\partial \mathbf{q}_2} \dot{\mathbf{q}}_1 \end{array}\right].
\end{aligned}
$$

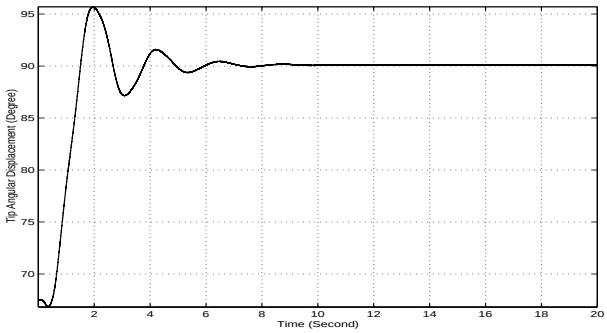

Figure 2: Tip trajectory for hybrid sliding mode by adaptive VSC.

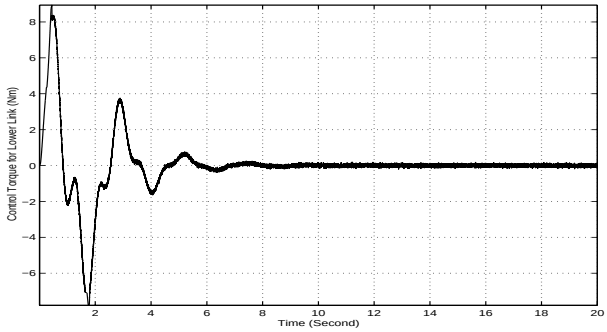

Figure 3: Lower link's control torque $\tau_1(t)$ for hybrid sliding mode by adaptive VSC.

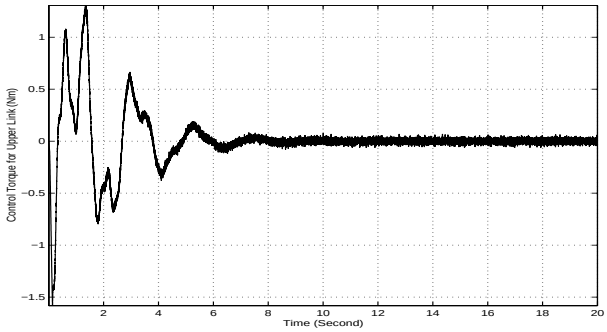

Figure 4: Upper link's control torque $\tau_2(t)$ for hybrid sliding mode by adaptive VSC.

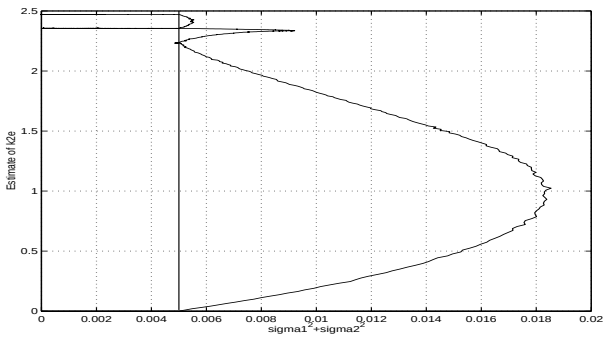

Figure 5: $\hat{k}_{2a}$ versus $\sigma_1^2 + \sigma_2^2$ by adaptive VSC with dead zone scheme, straight line stands for the size of dead zone.